Journal of Catalysis 274 (2010) 259–272

Contents lists available at ScienceDirect

Journal of Catalysis

journal homepage: www.elsevier.com/locate/jcat

Influence of the metal oxide support on the surface and catalytic properties of sulfated vanadia catalysts for selective oxidation of methanol

Hongying Zhao [a], Simona Bennici [a], Jingxuan Cai [b], Jianyi Shen [b], Aline Auroux [a,*]

[a] Université Lyon 1, CNRS, UMR 5256, IRCELYON, Institut de recherches sur la catalyse et l'environnement de Lyon, 2 Avenue Albert Einstein, F-69626 Villeurbanne, France
[b] Laboratory of Mesoscopic Chemistry, School of Chemistry and Chemical Engineering, Nanjing University, Nanjing 210093, China

ARTICLE INFO

Article history:
Received 27 April 2010
Revised 9 July 2010
Accepted 10 July 2010
Available online 11 August 2010

Keywords:
Supported vanadia catalysts
Acidity
Redox character
Ammonia adsorption calorimetry
Methanol selective oxidation
Dimethoxymethane

ABSTRACT

The selective oxidation of methanol to dimethoxymethane (DMM) was performed over a series of binary vanadia-based oxides (V_2O_5—TiO_2, V_2O_5—ZrO_2, V_2O_5—Al_2O_3 and V_2O_5—CeO_2) and the corresponding sulfated catalysts. The physicochemical properties of catalysts were characterized by BET, Raman, XPS, TPR–MS, ammonia adsorption calorimetry and sulfate TPD–MS techniques. The strength of the sulfate-support interaction depends on the nature of the oxide support and increases in the following order CeO_2 > Al_2O_3 > ZrO_2 > TiO_2. The catalytic reactivity was correlated with the nature of V—O-support bonds. Sample V_2O_5—TiO_2 exhibits the highest intrinsic activity of methanol oxidation. With the addition of sulfate, the selectivity to DMM was enhanced whereas the turnover frequency (TOF) value of vanadium sites decreased, with a rate depending on the strength of sulfate-support bonds. The best catalyst (V_2O_5—TiO_2—SO_4^{2-}) with higher DMM yield presented higher reducibility, proper acidity and moderate strength of sulfate species.

1. Introduction

Supported vanadia catalysts constitute a very important class of catalytic materials as they have started as model catalytic systems for fundamental studies of supported metal oxides and are extensively employed as commercial catalysts (selective catalytic reduction of NO_x with NH_3 to N_2 and H_2O, oxidative destruction of chlorinated hydrocarbons, oxidation of o-xylene to phthalic anhydride and selective oxidation and ammoxidation of C_1–C_4 hydrocarbons for olefins, oxygenates and nitriles) [1–6]. Supporting a metal oxide on the surface of another oxide was initially proposed to improve the catalytic activity of the active metal oxide phase due to a gain in surface area and mechanical strength. The support was first considered as an inert substance that provided a high surface to carry the active metal oxide component or to improve the mechanical strength of the catalyst material [7,8], but it can also behave as active phase if partly uncovered. Generally, supported vanadia catalysts may exhibit different catalytic properties since the metal oxide-support interaction affects both redox properties and dispersion of the active phase [9,10]. This is known as the metal oxide-support effect, although its exact origin and mechanism of operation is still unclear. The fundamental basis for the catalytic performances of supported vanadium oxides lies in the variability in geometric and electronic structure of surface vanadium oxides. Fundamental knowledge about the nature of supported vanadium oxides is of key importance in heterogeneous catalysis and spectroscopic tools are necessary to built up this knowledge.

Supported V_2O_5 catalysts are also widely studied in the reaction of methanol oxidation [11,12], which can be used as a probe reaction to characterize the activity of oxide catalysts [11,13] and further interpret it in terms of both structural and chemical (acidic and redox) properties. It appears from the literature that methanol can lead to different products by varying the nature of the catalyst and the reaction conditions (Scheme 1) [14–16]. Redox sites enable the production of partially oxidized species such as formaldehyde (HCHO, FA) or totally oxidized species (CO_2). Acidic sites enable condensation reactions, which can give dimethyl ether (CH_3OCH_3, DME), dimethoxymethane ($CH_3OCH_2OCH_3$, DMM) and methyl formate ($HCOOCH_3$, MF). Among the aforementioned products, DMM is especially interesting for industrial applications, since it is suitable as a fuel additive with a high stability. Further, it has been shown that the addition of SO_4^{2-} species to TiO_2 enhances the acidity and can lead to improving selectivity to DMM [17].

Therefore, in this work, as a sequel to studying the activity of methanol oxidation to DMM, sulfated vanadia-based oxides were evaluated by this reaction. The objective of the present investigation was to examine the influence of the host metal oxide on the acidic, redox and catalytic properties of vanadia and sulfated vanadia. Moreover, the effect of the host metal oxide on the nature of active VO_x phase and sulfate species was also investigated. The structural properties were characterized by Brunauer–Emmett–Teller (BET), inductively coupled plasma optical emission spectroscopy (ICP-OES), X-ray photoelectron spectroscopy (XPS) and

* Corresponding author. Fax: +33 472445399.
E-mail address: aline.auroux@ircelyon.univ-lyon1.fr (A. Auroux).

0021-9517/$ - see front matter © 2010 Elsevier Inc. All rights reserved.
doi:10.1016/j.jcat.2010.07.011

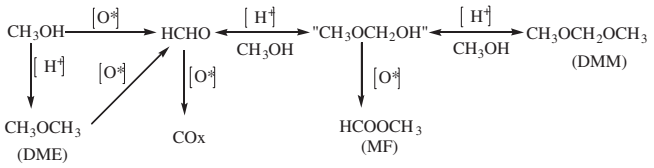

Scheme 1. Reaction pathways for the reaction of catalytic partial oxidation of methanol (adapted from Refs. [11,14]).

Raman spectroscopy and sulfate temperature-programmed desorption (TPD). The redox properties were examined by temperature-programmed reduction (TPR) coupled with mass spectrometer (MS) as a detector. In addition to this, the acidity of these catalysts was examined by using ammonia adsorption calorimetry.

2. Experimental

2.1. Catalyst preparation

The theoretical amount of vanadium pentoxide was fixed at 25 wt% whatever the host metal oxide used.

2.1.1. Prepared in two steps: co-precipitation of mixed oxides followed by ammonia sulfate impregnation

Binary vanadia-based oxides (denoted by VM(c1); M = Ti, Zr, Al and Ce) were prepared by modifying a previous reported co-precipitation method [18]. The vanadia, titania, zirconia, alumina and ceria precursors were $VOCl_3$, $TiCl_4$, $ZrOCl_2$, $Al(NO_3)_3$ and $Ce(NO_3)_3$, respectively. Briefly, $VOCl_3$ was dissolved into deionized water (1 mL $VOCl_3$ in 250 mL H_2O) mixed with 5–8 mL diluted HNO_3 (38 wt% HNO_3) with vigorous stirring to form a vanadium-containing solution (S1). The oxide-support precursor was dissolved into a limited deionized water to form the metal ion containing solution (S2), while $TiCl_4$ was dissolved in C_2H_5OH (1 mL $TiCl_4$ in 30 mL C_2H_5OH) in an ice bath. S2 was slowly dropped into S1 with continuous stirring to form a mixed solution (S3). Then, S3 solution was slowly dropped into diluted $NH_3{\cdot}H_2O$ placed in an ice bath to form the precipitate. The precipitate was first aged for 1 h at room temperature, then filtered, washed several times with deionized water until free from chloride ions and the filtrate cake dried as reported in [18]. The samples were all calcined at 673 K in air for 5 h, except for sample VAl(c1) which calcination temperature was increased up to 773 K for a better decomposition of the precursor.

The corresponding sulfated catalysts (denoted by VMS(c1-i); M = Ti, Zr, Al and Ce) were prepared by incipient wetness impregnation of the above mentioned supported vanadia catalysts with an aqueous solution containing the theoretical percentage of $(NH_4)_2SO_4$ to achieve a theoretical amount of 5 wt% SO_4^{2-} (1.7 wt% S). The resulting solids were then dried at 373 K overnight and then calcined at 673 K in air for 5 h.

2.1.2. Prepared directly by co-precipitation from sulfated precursors

Sulfated binary vanadia-based oxides (denoted by VMS(c2); M = Ti, Zr, Al and Ce) were also prepared by co-precipitation. The precursors were $VOSO_4$, $TiOSO_4$, $Zr(SO_4)_2$, $Al_2(SO_4)_3$ and $Ce(SO_4)_2$, respectively. The details of such preparation method have been previously described in [18]. Specifically, $Ce(SO_4)_2$ was dissolved in deionized water and then the pH was adjusted to around zero by adding dilute HNO_3 (38 wt% HNO_3) in order to complete the dissolution. Then, the aqueous solution of $VOSO_4$ was added dropwise to $Ce(SO_4)_2$ solution with vigorous stirring to form the mixed aqueous solution for precipitation with ammonia. At last, the samples were all calcined at 673 K in air for 5 h, except sample VAlS(c2) which calcination temperature was increased up to 773 K.

2.2. Catalyst characterization

Elemental analysis was performed using ICP optical emission spectroscopy (ICP–OES) with an ACTIVA spectrometer from Horiba JOBIN YVON.

The surface areas and pore sizes were measured by nitrogen adsorption at 77 K on a Micromeritics 2010 apparatus after heat pretreatment under vacuum for 3 h at a temperature 100 K lower than the calcination temperature.

The X-ray photoelectron spectra were measured on a KRATOS AXIS Ultra DLD spectrometer equipped with a hemispherical electron analyzer and an Al anode (Al Kα = 1486.6 eV) powered at 150 W, a pass energy of 20 eV and a hybrid lens mode. The detection area analyzed was 700 × 300 μm. Charge neutralization was required for all samples. The peaks were referenced to the C—(C, H) components of the C 1s band at 284.6 eV. Shirley background subtraction and peak fitting to theoretical Gaussian–Lorentzian functions were performed using an XPS processing program (vision 2.2.6 KRATOS). The residual pressure in the spectrometer chamber was 5×10^{-9} mbar during data acquisition.

Raman spectroscopy measurements were taken using a LabRAM HR (Jobin Yvon) spectrometer under ambient conditions. The excitation was provided by the 514.5 nm line of an Ar^+ ion laser (Spectra physics) employing a laser power of 100 μW. The laser beam was focused through microscope objective lenses (×100) down to a 1-micrometer spot on the sample.

H_2–TPR measurements were taken using a TPD/R/O−1100 instrument (ThermoFisher). Prior to each TPR run, the fresh sample was treated in a stream of O_2/He (0.998% v/v, flowing at 20 mL min^{-1}), ramping the temperature at 10 K min^{-1} from RT to 623 K and maintaining it for 60 min, and then cooled to 313 K. The TPR measurement was carried out using H_2/Ar (4.98% v/v) as reducing gas mixture, flowing at 20 mL min^{-1}. The heating rate was 5 K min^{-1} from 313 K to 1073 K. The H_2 consumption was detected by a thermal conductivity detector (TCD). The sample size used was adjusted in order to have around 69 μmol of V_2O_5 independently of the vanadia loading of the sample. This allowed us to maintain a K value of 100 s. The characteristic number K can be used to facilitate the selection of appropriate operating parameters: $K = S_0/(V^* C_o)$, where S_0 corresponds to current amount of reducible species (μmol), V^* relates to total flow rate of the reducing gas (cm^3(NTP)/s) and C_o is due to the current concentration of hydrogen at the reactor out (μmol/cm^3). A fixed K value between 60 and 140 s guarantees optimal conditions to obtain good TPR profiles [19,20]. The peak areas were calibrated with given H_2/Ar (4.98% v/v) mixture injections for TPR.

Gases evolving from the TPR reactor were analyzed by a mass spectrometer (Omnistar, Pfeiffer) with a heated capillary. The signals for m/e = 34 (H_2S) and 64 (SO_2) were recorded.

Temperature-programmed desorption (TPD) of sulfates was performed on a Setaram TG–DSC 111 device coupled with a mass spectrometer (Thermostar, Pfeiffer) as a detector. A capillary-coupling system was used. The TPD experiments were carried out in the range 298–923 K under helium flow as the carrier gas (35 mL min^{-1}). For each experiment, about 20 mg of sample with ammonia absorbed in previous microcalorimetric experiments was used. Initially, the samples were purged with helium at room temperature for 15 min and then heated with 5 K min^{-1} up to 373 K. The temperature was kept constant at 373 K for 30 min and then was linearly increased up to 923 K with same ramp of 5 K min^{-1}.

The microcalorimetric studies of ammonia adsorption were performed at 423 K in a heat flow calorimeter (C80 from Setaram)

linked to a conventional volumetric apparatus equipped with a Barocel capacitance manometer for pressure measurements. Ammonia used for measurements (Air Liquide, purity > 99.9%) was purified by successive freeze–pump–thaw cycles. About 100 mg of sample was pretreated in a quartz cell under evacuation overnight at a temperature 100 K lower than the calcination temperatures. The differential heats of adsorption were measured as a function of coverage by repeatedly introducing small doses of ammonia gas onto the catalyst until an equilibrium pressure of about 66 Pa was reached. The sample was then outgassed for 30 min at the same temperature, and a second adsorption was performed at 423 K until an equilibrium pressure of about 27 Pa was attained in order to calculate the irreversibly chemisorbed amount of ammonia at this pressure.

2.3. Catalytic reaction

The oxidation of methanol was carried out in a fixed-bed microreactor made of glass with an inner diameter of 6 mm. The methanol was introduced into the reaction zone by bubbling O_2/N_2 (1/5) through a glass saturator filled with methanol (99.9%) maintained at 278 K. In each test, 0.2 g of catalyst was loaded, and the gas hourly space velocity (GHSV) was 11,400 mL g^{-1} h^{-1}. The feed composition was maintained as methanol:O_2:N_2 = 1:3:15 (v/v). The tail gas out of the reactor was analyzed by an online gas chromatograph (GC) equipped with a flame ionization detector (FID) and a thermal conductivity detector (TCD). The column used was PORAPAK N for the separation of methanol, DMM and other organic compounds. The gas lines were kept at 373 K to prevent condensation of the reactant and products. The reaction was carried out at atmospheric pressure. Prior to the test, each catalyst was pretreated by heating in air at the same temperature as that used for calcination for 1 h and then cooled in the air flow to the reaction temperature.

3. Results and discussion

3.1. Structure properties

Table 1 shows the bulk composition and pore characteristics of the prepared materials. The sulfur content for all the VMS(c1-i) samples was similar, around 1.2–1.9 wt%, while the concentration of sulfur for VMS(c2) samples varied greatly and remained difficult to control since the different sulfated precursors. Samples VTi(c1), VZr(c1), VAl(c1) and VCe(c1) exhibited high surface area of 281, 334, 560 and 116 m^2 g^{-1}, respectively. Doping the VM(c1) samples with sulfate, a steady decrease in surface area can be seen for VMS(c1-i) samples, which might be due to the collapse of some pores during the second calcination. As example, the N_2 adsorption–desorption isotherms and pore size distribution of VMS(c1-i) samples are depicted in Fig. 1. The adsorption–desorption isotherms are similar to type IV and show type H1 or H3 hysteresis loop (mesoporous solid in which capillary condensation takes place at higher pressures of adsorbate in addition to multilayer adsorption at lower pressures), according to IUPAC classification [21]. Mean pores wideness of the oxides is centered around 11–20 nm of pore radius (Fig. 1 and Table 1). Quite often a mesoporous material contains also different amounts of micropores which result in larger adsorption at low adsorbate pressure followed by an adsorption profile resembling to type IV isotherm. The micropore surface area and the micropore volume were measured by using DeBoer's *t*-plot analysis. Most of the catalysts show some microporosity, especially for VAl(c1) and VAlS(c1-i) samples. VMS(c2) samples, simply prepared by co-precipitation, display similar surface area and porosity data as VMS(c1-i) samples.

The Raman spectra of binary vanadia-based catalysts and corresponding sulfated catalysts are shown in Fig. 2. As presented in Fig. 2a, pronounced Raman bands at 1027 cm^{-1} assigned to terminal V=O bond and at 933 cm^{-1} due to V—O—V linkage for polymeric vanadate species were detected for all samples, regardless of whether SO_4^{2-} was added or not and whatever the preparation method used [22–24]. No V—O-support bridging bonds were observed probably because of the formation of V—O—V bridges of polymeric vanadia species by breaking V—O—Ti bonds of the monomeric vanadyl species, $(Ti—O)_3V=O$ [25], which implies a weak strength V—O—Ti bond. The bands at 639, 517 and 404 cm^{-1} are corresponding to Ti—O groups [26]. A similar phenomenon was observed for VZr and VZrS samples, as shown in Fig. 2b. A weak Raman band present at 1024 cm^{-1} can be associated to the terminal monooxo V=O bond of surface VO_4 species [27]. Broad Raman bands at 918 cm^{-1} with a small left-hand shoulder at ~801 cm^{-1} are corresponding to the υ_{as} vibration of bridging V—O-zirconia bonds [28] and bridging V—O—V bonds [1–3], respectively. No Raman bands corresponding to zirconium oxide were detected. The Raman spectra for VAl and VAlS samples are presented in Fig. 2c. This high surface area VAl(c1) sample does not give rise to any Raman active bands for alumina support in agreement with the literature [29], and consequently all the observed Raman bands originate from the supported vanadia

Table 1
Chemical analysis and pore characteristics of supported vanadia catalysts.[a]

Sample	$T_{calcination}$ (K)	CA (wt%)			Surface area (m^2 g^{-1})		Pore volume (cm^3 g^{-1})		Pore diameter (nm)
		V	Ti/Zr/Al/Ce	S	S_{BET}	S_{micro}	V_{BJH}	V_{micro}	d_{BJH}
VTi(c1)	673	13.7	41.8	–	281	3.6	1.02	1.02	11.3
VTiS(c1-i)	673	13.1	40.5	1.5	204	5.5	0.82	0.82	11.9
VTiS(c2)	673	12.3	38.2	1.8	282	–	0.75	–	9.0
VZr(c1)	673	10.0	49.9	–	334	–	0.85	–	9.8
VZrS(c1-i)	673	9.9	49.1	1.9	277	4	0.75	–	10.2
VZrS(c2)	673	14.4	48.7	0.8	321	14	1.13	0.003	14.2
VAl(c1)	773	9.9	33.8	–	560	28	3.21	0.01	20.4
VAlS(c1-i)	673	9.9	33.5	1.2	392	26	1.23	0.01	10.4
VAlS(c2)	773	8.8	27.4	5.6	405	17	1.91	0.004	18.9
VCe(c1)	673	14.0	59.4	–	116	0.8	0.44	–	13.8
VCeS(c1-i)	673	13.4	55.9	1.9	86	6	0.37	–	15.1
VCeS(c2)	673	14.5	55.2	1.2	73	14	0.24	0.005	18.2

[a] S_{BET} is the surface area calculated by the BET method; V_{BJH} and d_{BJH} are the cumulative adsorption pore volume and pore diameter, respectively (1.7 < pore diameter < 300 nm), calculated by the BJH method; S_{micro} and V_{micro} are respectively the surface area and pore volume in the micropore range (pore diameter < 2 nm) calculated by the DeBoer's *t*-plot method.

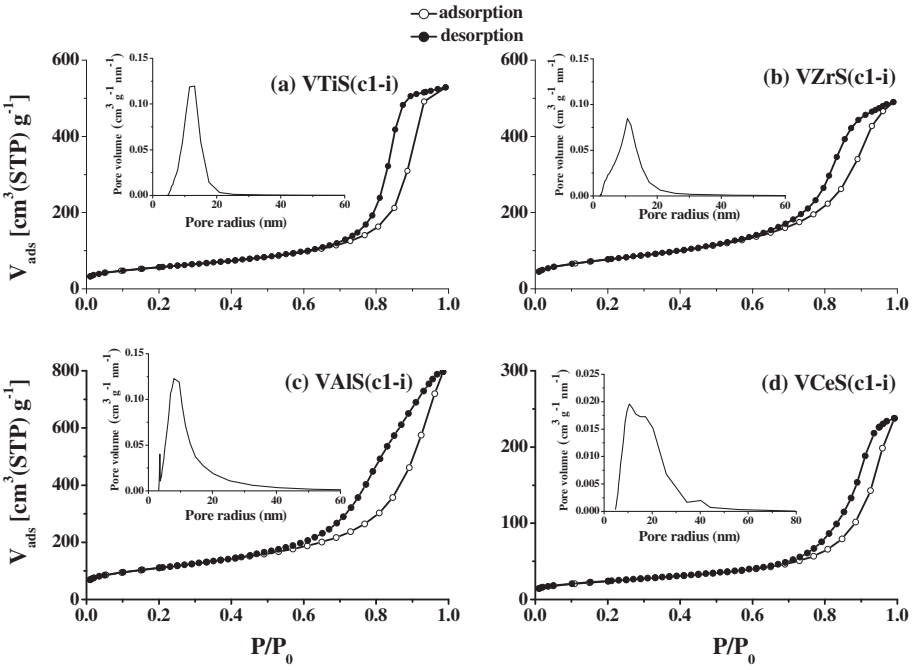

Fig. 1. N_2 adsorption–desorption isotherms of sulfated supported vanadia catalysts. (Inset: pore radius distribution curve from the desorption branch of the isotherms.)

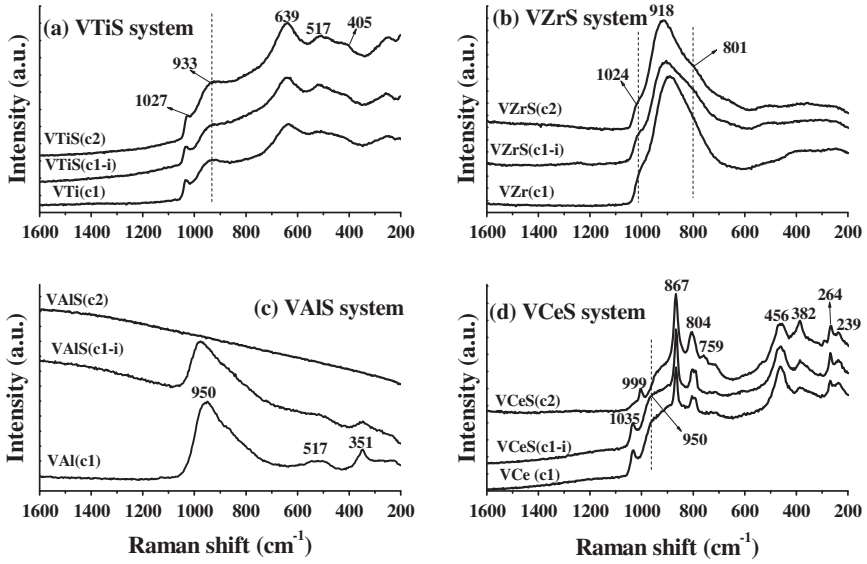

Fig. 2. Raman spectra of (a) VTiS samples, (b) VZrS samples, (c) VAlS samples and (d) VCeS samples.

phase. The Raman bands at ~517 and 351 cm^{-1} have previously been assigned to the bridging V—O—V bonds of the monomeric and polymeric surface VO_4 species [27,30]. The broad band at ~950 cm^{-1} has recently been assigned to bridging V—O-alumina based on density functional theoretical (DFT) calculation [28]. No bands corresponding to monooxo V=O vibration were observed. The difference between our results and those of Wachs et al. [31,32] can be explained by working under nondehydrated conditions. Moreover, our samples were prepared by a co-precipitation method which could favor the formation of V—O—Al bonds.

Doping with SO_4^{2-} species seems to perturb the molecular structure of the surface vanadia species by broadening Raman bands for sample VAlS(c1-i). Additionally, no Raman band was observed for sample VAlS(c2) containing higher content of sulfur, suggesting that the vanadia species are totally coated by alumina or sulfate species.

As shown in Fig. 2d, the Raman bands at 456 and 239 cm^{-1} are due to CeO_2 [33]. In addition to the CeO_2 features, VCe(c1) and VCeS(c1-i) samples show similar Raman band to VTiS samples at 1035 and 950 cm^{-1}. The bands at 867, 804, 759, 456, 382 and 264 cm^{-1} are characteristic of bulk $CeVO_4$ [34,35]. The formation of CeVO4 compound somehow reflects the presence of V—O—Ce bonds. The XPS measurements presented in the latter paragraphs provide more information about the formation of Ce^{3+} ions, supporting this observation. Trace feature of crystalline V_2O_5 species is present only in sample VCeS(c2) at 999 cm^{-1}, possibly due to the relatively low surface area.

To understand the nature of interactions between ceria and dispersed surface vanadia species, samples of VCe and VCeS have been investigated by XPS technique. The photoelectron peaks of O 1s and Ce 3d pertaining to these VCe and VCeS samples are depicted in Figs. 3 and 4, respectively. The results of surface elemental analysis, binding energies of V $2p_{3/2}$, Ce $3d_{5/2}$, O 1s and S $2p_{1/2}$, as well as the relative components from the decomposition of the O 1s lines are presented in Table 2. As can be noted from Table 2, the XPS results of surface vanadium, cerium and sulfur composition are consistent with chemical analysis results. Additionally, the lower vanadium composition for sample VCeS(c2) is possibly due to the higher concentration of $CeVO_4$ (confirmed by the intensity of XRD patterns corresponding to $CeVO_4$), since surface vanadia may diffuse into the ceria lattice. The binding energies of V $2p_{3/2}$ for all the VCe and VCeS samples were ~517.2 eV, indicating that the vanadia surface species were fully oxidized (oxidation state V^{5+}) [36]. The S $2p_{1/2}$ line at the binding energy of about 169.0 eV is typical of sulfur in S^{6+} oxidation state in the form of SO_4^{2-} species on the surface of metal oxides [37,38].

As shown in Fig. 3, the O 1s peaks are, in general, broad and complicated because of the overlapping contribution of oxygen from the various component oxides, which could be divided into three bands. The quantitative results acquired from the theoretical Gaussian–Lorentzian functional peak fitting are presented in Table 2 and agree with the value reported in a previous paper [18]. In addition, the peak centered at 532.0–532.2 eV in this work can be attributed both to $CeVO_4$ compound [39] and sulfate species.

The XPS core-level spectra of Ce 3d are generally characterized by complex but distinct features that are related to the final-state occupation of the Ce 4f level [40]. According to the literature [41,42], the Ce 3d spectrum can be assigned as follows: the peaks labeled u are due to $3d_{3/2}$ spin–orbit states, and those labeled v are corresponding to $3d_{5/2}$ states. Specially, the u'''/v''' doublet is due to the primary photoemission from Ce(IV)-O_2. The u/v and u''/v'' doublets are shakedown features generating from the transfer of one or two electrons from a filled O 2p orbital to an empty Ce 4f orbital. The u'/v' doublet is due to photoemission from Ce(III) cations. Therefore, the Ce 3d spectra of all VCe and VCeS samples shown in Fig. 3 revealed a mixture of Ce^{3+} and Ce^{4+} oxidation states. In fact, cerium in $CeVO_4$ was in the valence +3. Thus, the XPS results concerning the formation of $CeVO_4$ compound support the conclusions drawn from Raman results fairly well.

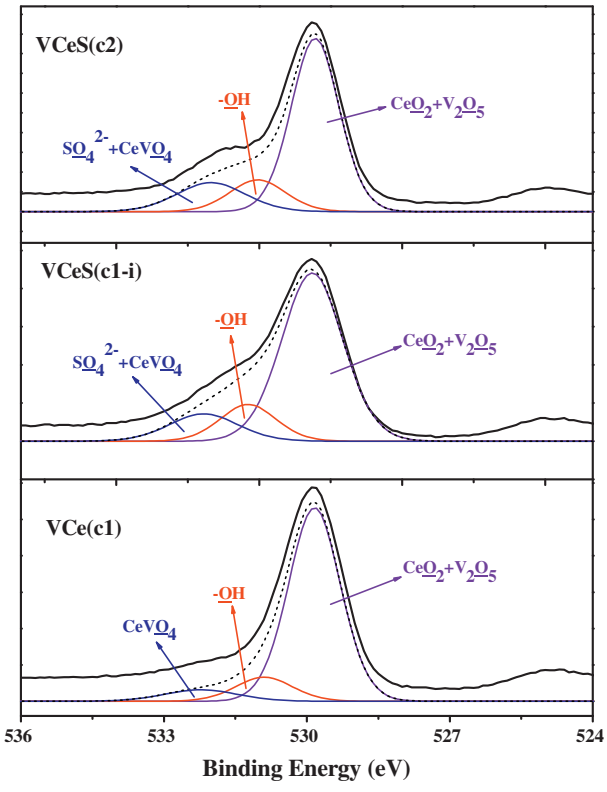

Fig. 3. O 1s XPS spectra of VCe and VCeS samples (experimental O 1s spectrum: black straight line, simulated O 1s spectrum by the contribution of oxygen from various component oxides: black dotted line, O 1s spectrum of V_2O_5 and CeO_2 oxides: violet, O 1s spectrum of surface hydroxyl groups: red, O 1s spectrum of SO_4^{2-} species and $CeVO_4$ compound: blue). (For interpretation of the references to colors in this figure caption, the reader should refer to the web version of the article.)

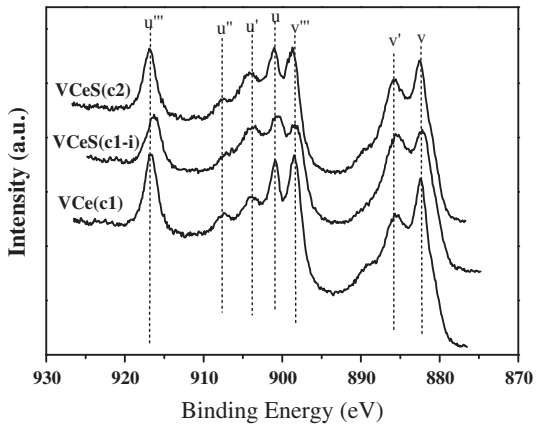

Fig. 4. Ce 3d XPS spectra of VCe and VCeS samples.

3.2. Surface acidity

Among the surface properties of vanadia catalysts of some importance for their catalytic activity in selective oxidation, acidity is one of the most significant [43]. The acidity measurements were taken by means of NH_3 adsorption experiments monitored by calorimetry coupled to volumetry. For each experiment, the equilibrium pressure P, the adsorbed NH_3 amount n_a, and the corresponding evolved heat Q_{int} were recorded, and then these data were expressed in different ways to evaluate the surface acidity, such as the volumetric isotherms (n_a, P) and the variation of the differential heats Q_{diff} as a function of n_a. The differential heat of adsorption Q_{diff} (or adsorption enthalpy ΔH_{ads}) is related to integral heat by the formula $Q_{diff} = \partial Q_{int}/\partial n_a$ [43]. Table 3 summarizes the main results obtained. Fig. 5 shows the plots of the differential heats of NH_3 adsorption as a function of NH_3 coverage and Fig. 6 presents the ammonia adsorption isotherms for the series of binary vanadia-based catalysts and corresponding sulfated catalysts.

The Q_{diff} values as exhibited in Fig. 5 are all similar with a sharp decrease at the beginning except for sample VTiS(c1-i) due to sulfate species which can increase or decrease the acidity at low coverage. The surfaces of these catalysts appear as heterogeneous with a continuous slowly decrease in the acidity as a function of the coverage.

SO_4^{2-} addition increased the acidity for all the samples, as can be easily seen on the isotherms (Fig. 6). For the VZr and VAl samples, a clear trend was observed: the more SO_4^{2-} was added, the more the acidity increased. On the other hand, for the VTi system, sample VTiS(c1-i) with 1.5 wt% S exhibited higher acidity than sample VTiS(c2) containing 1.8 wt% S. This behavior might be related to the higher concentration of vanadium species in sample VTiS (c1-i), which can improve the acidity of the system. Similarly, for the VCe system the acidity trend was not following the SO_4^{2-} content,

Table 2
X-ray photoelectron spectroscopy analysis, binding energies of surface species and O 1s concentration (in at%) for different oxygen species ($V_2O_5 + CeO_2$; —OH; $SO_4^{2-} + CeVO_4$) present on the VCe and VCeS catalysts surfaces.

Sample	XPS (wt%)			Binding energy (eV)					
	V	Ce	S	V $2p_{3/2}$	Ce $3d_{5/2}$-satellite	O 1s			S $2p_{3/2}$
VCe(c1)	14.9	57.6	–	517.2	882.5–916.9	529.8(82%)[a]	530.9(11%)[b]	532.2(7%)[c]	168.5
VCeS(c1-i)	14.1	53.0	1.8	517.1	882.4–916.8	529.9(72%)[a]	531.2(15%)[b]	532.1(13%)[c]	–
VCeS(c2)	11.7	59.8	1.4	517.2	882.3–916.3	529.8(69%)[a]	531.0(15%)[b]	532.0(16%)[c]	168.8

[a] Binding energies (BEs) between 529.8 and 529.9 eV correspond to O in CeO_2 and V_2O_5.
[b] Binding energies (BEs) between 530.9 and 531.2 eV correspond to O in —OH.
[c] Binding energies (BEs) between 532.0 and 531.2 eV correspond to O in SO_4^{2-} and $CeVO_4$.

Table 3
Calorimetric data for ammonia adsorption at 423 K and corresponding TPD data on VM and VMS catalysts.

Sample	V_{total}[a] (μmol g^{-1})	V_{total}[a] (μmol m^{-2})	V_{irrev}[b] (μmol g^{-1})	V_{irrev}[b] (μmol m^{-2})	Q_{init}[c] (kJ mol^{-1})	T_{max}[d] SO_4^{2-} (K)	
						Peak 1	Peak 2
VTi(c1)	461	1.64	210	0.75	180	n.d.[e]	n.d.[e]
VTiS(c1-i)	501	2.46	311	1.52	7	676	767
VTiS(c2)	549	1.95	292	1.04	210	687	765
VZr(c1)	555	1.66	310	0.93	204	n.d.[e]	n.d.[e]
VZrS(c1-i)	530	1.91	288	1.04	194	741	867
VZrS(c2)	573	1.79	319	0.99	257	765	852
VAl(c1)	420	0.75	188	0.34	195	n.d.[e]	n.d.[e]
VAlS(c1-i)	461	1.17	232	0.59	207	966	n.d.[e]
VAlS(c2)	591	1.46	318	0.79	174	964	n.d.[e]
VCe(c1)	205	1.77	64	0.55	187	n.d.[e]	n.d.[e]
VCeS(c1-i)	165	1.92	55	0.64	159	>973	n.d.[e]
VCeS(c2)	183	2.51	82	1.12	151	>973	n.d.[e]

[a] Amount of NH_3 adsorbed under an equilibrium pressure of 27 Pa.
[b] Amount of irreversible chemisorbed NH_3.
[c] Heat evolved from the first ammonia dose.
[d] Maximum temperature of SO_4^{2-} decomposition peak from TPD–MS.
[e] Not determined.

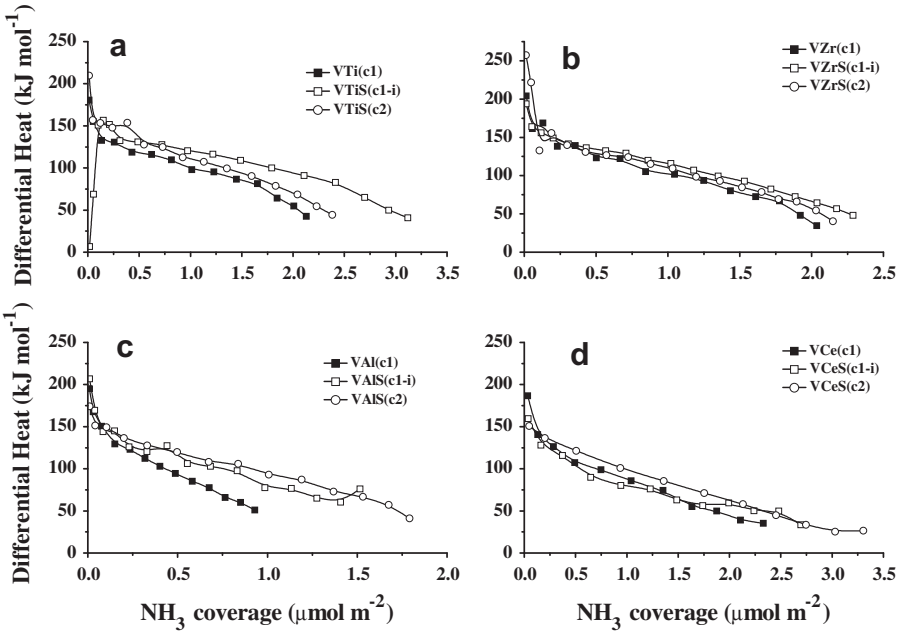

Fig. 5. Differential heats of ammonia adsorption versus the adsorbed amount on (a) VTiS samples, (b) VZrS samples, (c) VAlS samples and (d) VCeS samples.

and the acidity varied in the order: VCeS(c2) > VCeS(c1-i) > VCe(c1). This trend was related to the formation of $CeVO_4$, which increases the acidity of VCe samples, CeO_2 being mainly a basic support. This observation was confirmed by the increasing intensity of XRD patterns of $CeVO_4$, which were the strongest for sample VCeS(c2). Additionally, the number of acid sites of these catalysts (both the total population, $V_{NH_3,total}$, and that of strong sites, $V_{NH_3,irrev}$) reported in Table 3 follows the same trend.

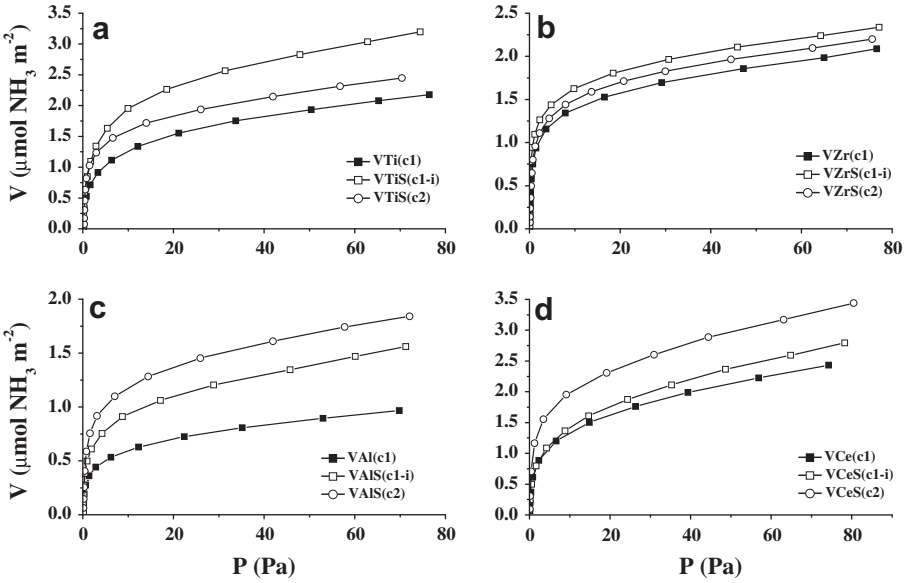

Fig. 6. Volumetric isotherms of NH_3 adsorption at 423 K for (a) VTiS samples, (b) VZrS samples, (c) VAlS samples and (d) VCeS samples.

To obtain more detailed information on the acidity and thermal stability of catalysts, simultaneous TPD–MS–TG–DSC profiles of sulfated binary vanadia-based catalysts are shown in Fig. 7. As presented in TG curves, the first weight loss step, in all cases, is mostly caused by ammonia desorption. Another remarkable weight loss in the higher temperature range corresponding to liberation of SO_4^{2-} is observed simultaneously with endothermic feature especially for VTiS and VZrS samples. Moreover, the weak endothermic peaks are possibly the overlay of the endothermic peak of sulfate desorption and exothermic crystallization peak.

The maximum temperatures of TPD peaks for desorbing sulfate species are summarized in Table 3. The used samples were those previously analyzed by ammonia adsorption calorimetry. Because it would not be accurate to rank the acid strengths by simply comparing the ammonia desorption maxima, due to complex diffusion effects, especially for porous materials, the ammonia desorption peaks are not commented in this paper.

In a previous paper [44], a strange phenomenon of low initial heat of adsorption was observed by ammonia calorimetry on few sulfated vanadia–titania samples. This phenomenon, interpreted by an endothermic reaction associated to an exothermic adsorption, was also obtained in this work but only for VTiS(c1-i) sample. Although the low heats of adsorption were explained well as the contribution of the interaction of dissociated ammonia with sulfates [45], the desorption behavior of sulfate species obtained from TPD indicates a reasonable explanation for what kinds of sulfate materials could favor the low initial heat of adsorption.

By using TG–TPD–MS, we have determined that the primary products of sulfated metal oxides thermal decomposition are SO_2 and O_2, which is consistent with previously reported mass spectrometry results [46]. As shown in Fig. 7 and Table 3, sample VTiS(c1-i) exhibited a main peak centered at 676 K with a small shoulder at 767 K, while sample VTiS(c2) presented a peak with two maxima at 687 and 765 K. This behavior suggests the existence of different structures of sulfate species, expecting that one desorption profile could be pertained to one sulfate structure only. Besides, as proposed before by Waqif et al. [47] based on IR studies, only one sulfate type of $(-O)_3S{=}O$ was found on TiO_2. Therefore, we attempt to say that the sulfate desorption peak centered at 676 K could possibly be assigned to bisulfate and/or lowly polymerized species while the shoulder at 767 K corresponded to highly polymerized species. In addition, the intensity of the peak centered around 767 K is much higher for sample VTiS(c1-i) compared to VTiS(c2), implying a higher content of weak sulfate species for sample VTiS(c1-i).

In the case of VZrS, VAlS and VCeS systems, similar sulfate desorption peaks were observed for each system regardless the preparation method and sulfate density. For VZrS samples, the first small peak is placed at relatively low-temperature (~741 K) corresponding to lowly polymerized species, while the second peak centered at ~867 K is assigned to highly polymerized species. Additionally, samples VAlS and VCeS exhibited only one desorption sulfate peak at higher temperatures of ~960 K and >973 K, respectively, possibly due to the highly polymerized sulfate species. In conclusion, the maximum temperature of releasing sulfate species varied in the order of VTiS < VZrS < VAlS < VCeS, implying that the strength of sulfate-support interaction strongly depends on the oxide support (TiO_2, ZrO_2, Al_2O_3 and CeO_2).

It is noteworthy that VTiS(c1-i) sample which presented low initial heat of adsorption simultaneously contained higher concentration of weak sulfate species. These results confirmed that not all the sulfated materials can induce this strange phenomenon of low initial heat of adsorption at low ammonia coverage, but only samples possessing enough weak sulfate species, such as bisulfate and low polymerized sulfate species.

3.3. Redox properties

To investigate the effect of oxide support (TiO_2, ZrO_2, Al_2O_3 and CeO_2) on the redox properties of the studied catalysts, the TPR technique was employed and the reduction process was monitored by mass spectrometry.

Fig. 8a–d shows the TPR profiles in the temperature range of 350–1050 K for all the samples. As shown in Fig. 8a, sample VTi(c1) displays a peak centered at ~708 K with a right-hand shoulder maximizing around 758 K. The TPR profile of sample VTi(c1) indicates that the majority of vanadia species are present as polymeric VO_x species (T_{m1} < 760 K) [48,49], as evidenced by Raman spectra. With the addition of SO_4^{2-}, samples VTiS(c1-i) and VTiS(c2) exhibit a peak maximizing around 760 K with a left-hand shoulder at 728 K. As already reported by other authors [50,51], the reduction of S(VI) species could affect the shape of H_2 consumption profile,

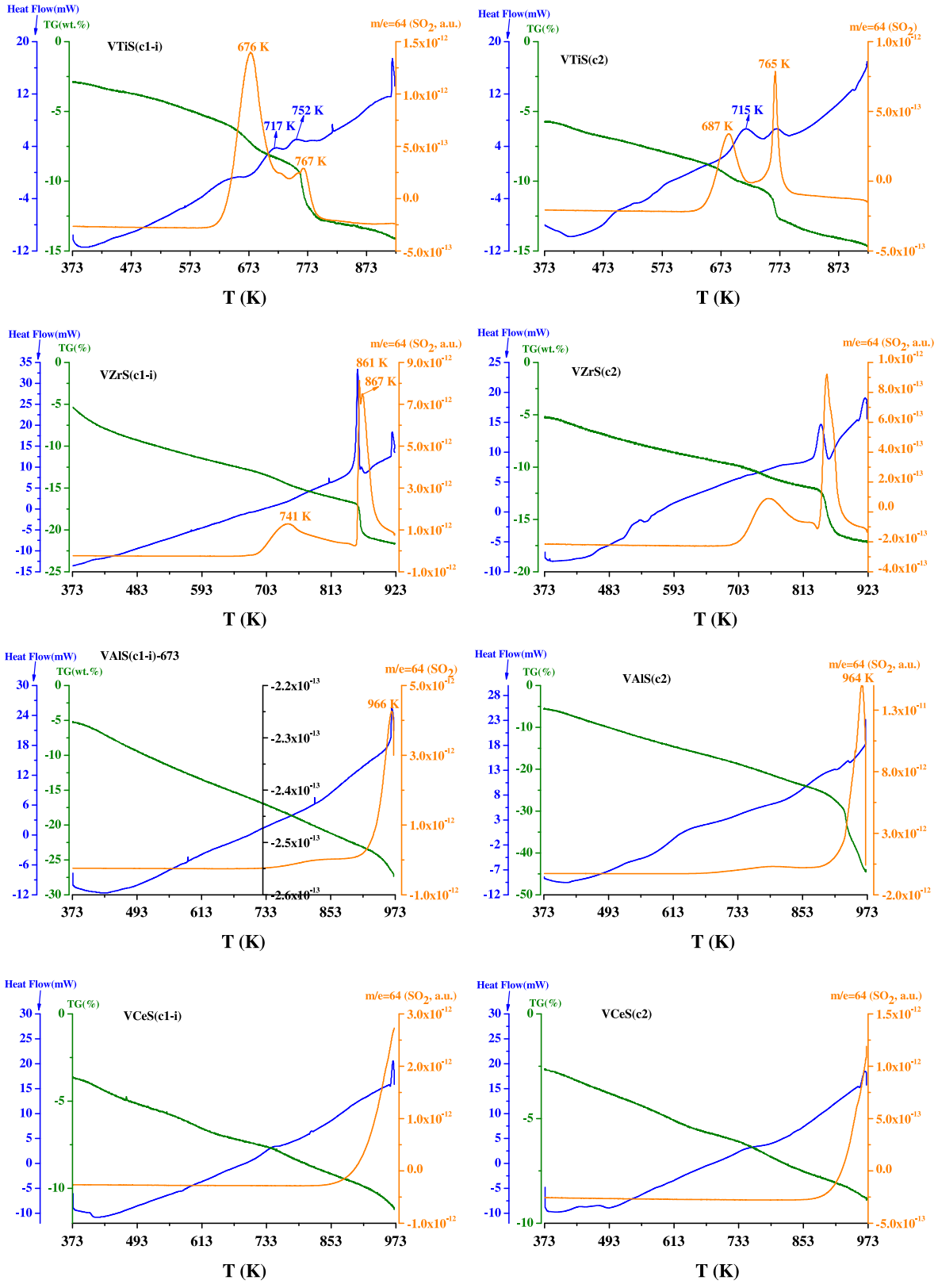

Fig. 7. Simultaneous TPD–MS–TG–DSC profiles (TG: green, DSC: blue, m/e = 64: orange) for supported vanadia catalysts. (For interpretation of the references to colors in this figure caption, the reader should refer to the web version of the article.)

which was checked by mass spectrometry as reported in the following paragraphs. There is another small peak at much higher temperature, in the range of 900–1030 K, possibly assigned to bulk V_2O_5 issued from the same polymeric VO_x species.

The reduction behavior of VZr and VZrS samples is illustrated by Fig. 8b. Only one peak with a maximum at 742 K was observed for sample VZr(c1), whereas samples VZrS(c1-i) and VZrS(c2) present a sharp peak centered at ~762 K and superimposed with a small

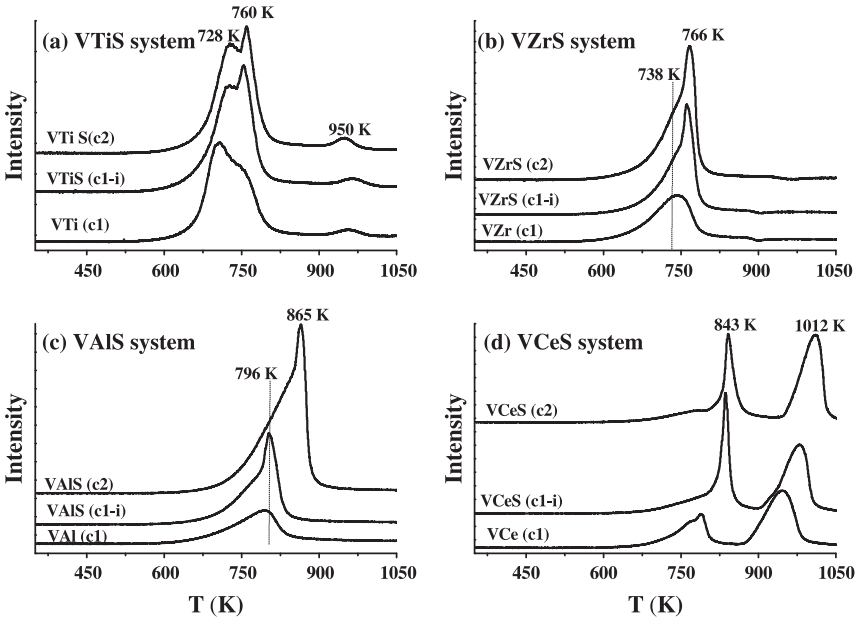

Fig. 8. TPR profiles of (a) VTiS samples, (b) VZrS samples, (c) VAlS samples and (d) VCeS samples.

left-hand shoulder (~738 K). By analogy with VTiS samples, most vanadia species render as polymeric VO_x phase. As shown in Fig. 8c for VAl and VAlS samples, the maximum temperature of the reduction peak (T_{m1}) shifts to higher values and the intensity of TPR peak increases by adding sulfate species, especially for sample VAlS(c2) possessing 5.6 wt% S.

The TPR profiles of VCe and VCeS (c1-i and c2) samples are shown in Fig. 8d. Two distinct reduction peaks can be observed for these three samples (see Table 4). As reported in the literature [33], pure CeO_2 shows two reduction peaks at 795 and 981 K, indicative of the reduction of Ce^{4+} to Ce^{3+}. The reduction peak for VCe(c1) is at 790 K, suggesting that the addition of vanadium oxide to ceria obscures the low-temperature peak. This is consistent with the stabilization of Ce^{3+} sites at the vanadia–titania interface [52]. Upon the addition of sulfate, the maximum temperature of TPR peak shifts to 837 K for VCeS(c1-i) and to 843 K for VCeS(c2). There is some Ce^{3+} ($CeVO_4$) at the vanadia–ceria interface, confirmed by the Raman and XPS measurements. The formation of $CeVO_4$ out of surface vanadium oxide on CeO_2 reveals that V enters the ceria lattice or that ceria ions migrate to surround vanadia, in a strong metal-support interaction-like behavior. Thus, the first reduction peak (~790 K) would be indicative of the reduction of $V^{5+}O_x$/$Ce^{4+}O_2$ to $Ce^{3+}V^{5+}O_4$/$Ce^{4+}O_2$ (the reductive formation of $CeVO_4$) and not of the reduction of surface vanadia species [53]. Bulk $CeVO_4$ exhibits a reduction peak at 954 K due to $V^{5+} \rightarrow V^{3+}$ transformation and bulk CeO_2 exhibits an intense second reduction maximum at 981 K. Therefore, the second peak of mixed vanadia–ceria samples (~948 K) must be a linear combination of the reduction maxima of CeO_2 and of the transformation of V^{5+} to V^{3+} in the $CeVO_4$ phase.

The T_{m1} value of the studied samples increases in the order of VTi (708 K) < VZr (742 K) < VCe (790 K) < VAl (796 K), suggesting that the most reducible nature of TiO_2 and ZrO_2 surfaces typically leads to more reducible oxide domains than the refractory Al_2O_3 and CeO_2 supports.

The mass spectrometry (MS) data for VMS(c1-i) systems (M = Ti, Zr, Al and Ce), obtained after the TPR runs, are exhibited in Fig. 9a–d. Mass data show that twin reduction peaks correspond to the reduction of S^{6+} species (SO_4^{2-}) to S^{4+} (SO_2) and to S^{2-} (H_2S) species, respectively. In case of sample VTiS(c1-i), no formation of

Table 4
Reducibility of the catalysts as revealed by the H2–TPR measurements.

Catalyst	T_{max} (K)[a]			Consumption H_2 (mmol g^{-1})	T_{max}[b] (K)		
		Peak 1 (T_{m1})	Peak 2 (T_{m2})		SO_2	H_2S	
VTi(c1)	758	708	963	2.0	–	–	
VTiS(c1-i)	724	754	965	2.3	700	n.d.[c]	
VTiS(c2)	728	760	950	2.3	–	–	
VZr(c1)		742	n.d.[c]	1.4	–	–	
VZrS(c1-i)	738	762	n.d.[c]	1.9	732	767	
VZrS(c2)	738	766	n.d.[c]	2.2	–	–	
VAl(c1)		796	n.d.[c]	1.4	–	–	
VAlS(c1-i)	781	805	n.d.[c]	2.0	761	802	
VAlS(c2)	843	865	n.d.[c]	4.0	–	–	
VCe(c1)		790	948	3.0	–	–	
VCeS(c1-i)		837	980	3.5	817	836	974
VCeS(c2)		843	1012	3.4	–	–	

[a] Maximum temperature of the H_2–TPR peaks.
[b] Maximum temperature of SO_4^{2-} reduction peaks from TPR–MS.
[c] Not determined.

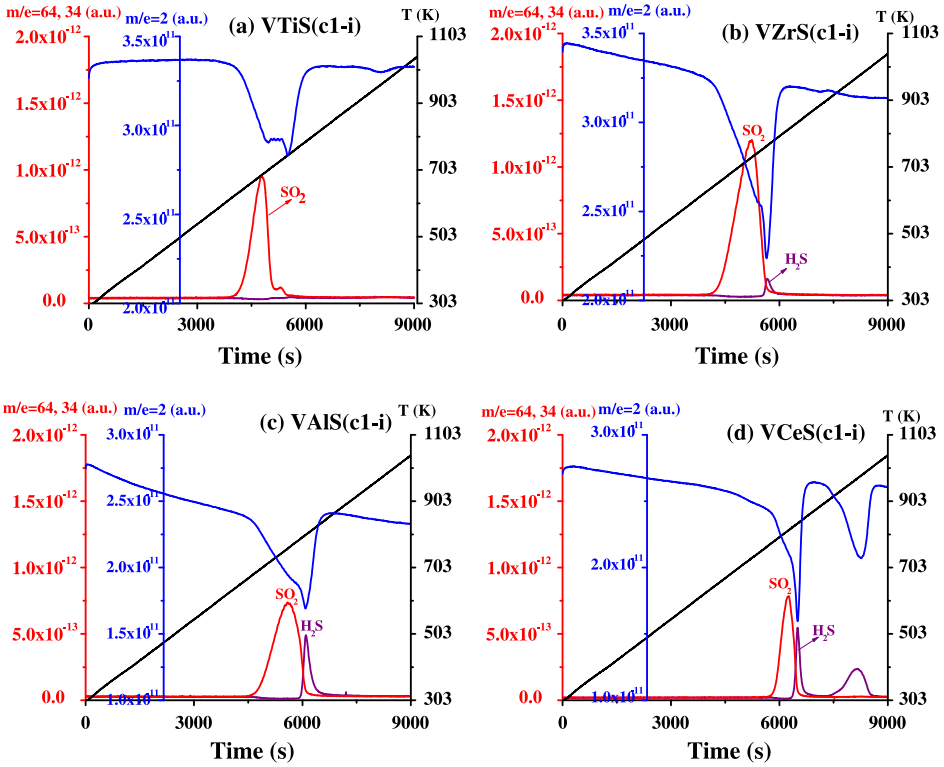

Fig. 9. Mass spectra of the gases evolved during the TPR analysis for (a) VTiS(c1-i), (b) VZrS(c1-i), (c) VAlS(c1-i) and (d) VCeS(c1-i) samples (m/e = 64: red; m/e = 34: violet; m/e = 2: blue; temperature: black). (For interpretation of the references to colors in this figure caption, the reader should refer to the web version of the article.)

H_2S was detected, whereas the other samples show the presence of both H_2S and SO_2. The major SO_2 peak for sample VTiS(c1-i) is observed between 604 and 779 K with a maximum at 700 K. Together with H_2 consumption profile as shown in Figs. 8a and 9a (m/e = 2), the small shoulder obtained at 724 K for sample VTiS(c1-i) (Fig. 8a) can be attributed to the reducing of sulfate species since it matches the SO_2 evolution very well. In another word, the main peak at 754 K is mostly assigned to dispersed VO_x species. These results reflect that the addition of sulfate inhibits the reduction of vanadia since the reduction peak maxima slightly shift from 708 K for VTi(c1) to 754 K for VTiS(c1-i).

For sample VZrS(c1-i), two sulfate reduction products (H_2S and SO_2) were detected but did not evolve in parallel in the whole temperature range. The first peak is in the temperature range of 628–780 K with maximum yield at ~730 K and is due to SO_2. Beyond 751 K, H_2S evolution is observed, but this peak is very small. A similar phenomenon was observed for VAlS(c1-i) and VCeS(c1-i) samples. MS analysis shows two distinct features: a low-temperature peak related to SO_2 formation (a peak centered at 762 K for VAlS(c1-i) and 815 K for VCeS(c1-i)), followed by a higher temperature peak related to H_2S formation. Specially for sample VCeS(c1-i), two peaks for H_2S release with maxima at 836 K and 974 K were observed (see Table 4). All the SO_2 and H_2S evolutions matched that of H_2 consumption.

The sulfate reduction temperature for liberating SO_2 and H_2S is in respect with the nature of oxide support and decreases in the order of VTiS < VZrS < VAlS < VCeS. Again, the different observed maxima and relative intensity of these two distinct SO_2 and H_2S peaks indicate different types of sulfate species conforming to different sulfate structures [54,55]. The sulfate species reduced at low-temperature could correspond to those not strongly bonded to the surface and consequently should be readily reduced to SO_2, while the sulfate species reduced at higher temperature are interacting strongly with the surface, and thus should be more prone to be reduced to H_2S, since SO_2 cannot be formed without breakage of a M—O bond (M = Ti, Zr, Al and Ce). This observation is consistent with the thermal stability of sulfate species present on different oxide supports, as indicated by TPD–MS measurements.

As reported in Table 4, VCe and VCeS samples exhibit the highest H_2 consumption implying higher concentration of redox sites since both V and Ce oxides possess redox sites. Moreover, H_2 consumption increased upon addition of sulfate, especially for sample VAlS(c2) with 5.6 wt% S.

3.4. Methanol oxidation reaction

It is now well admitted that the partial oxidation of methanol is strongly sensitive to the nature of the active sites, which can be employed to provide information about the surface acidity and redox properties simultaneously [11,14]. Fig. 10A–D shows the whole catalytic performance of samples, while Table 5 presents the turnover frequency of catalysts, which is defined as the number of methanol molecules converted per surface vanadium oxide site per second [32].

As shown in Fig. 10A, sample VTi(c1) exhibited high activity. For example, the conversion of methanol was 58% at 393 K, with selectivities to DMM, FA, MF and DME of 64%, 15%, 21% and 0%, respectively. Moreover, the distribution of products indicates that the surface acidity was not strong enough to effectively catalyze the reaction of FA condensation with methanol to produce DMM, leading to the production of oxidation products (MF and FA). With increasing reaction temperature, the selectivity to DMM decreased while the selectivity to FA and MF increased, with a rapid increase in the total conversion of methanol. The sudden drop in DMM selectivity is possibly as a result of thermodynamic constrains for DMM synthesis [14]. At 413 K, the conversion of methanol dramatically increased to 95%, and only oxidation products could be observed, with selectivities to FA, MF and CO_x of 10%, 61% and 28%,

Table 5
The turnover frequencies (TOFs) and characteristics of supported vanadia and sulfated supported vanadia catalysts.[a]

Sample	N_s[b] (V nm^{-2})	Monolayer surface V loading[c] (V nm^{-2})	Conversion of methanol (%) at 393 K	TOF[d] $\times 10^4$ (s^{-1})
VTi(c1)	5.8	7.9 [26]	58	15.9
VTiS(c1-i)	7.6		42	12.1
VTiS(c2)	5.2		37	11.3
VZr(c1)	3.5	6.8 [26]	11	4.2
VZrS(c1-i)	4.2		9	3.5
VZrS(c2)	5.3		8	2.1
VAl(c1)	2.1	7.3 [26]	1	0.4
VAlS(c1-i)	3.0		1	0.4
VAlS(c2)	2.6		2	0.9
VCe(c1)	14.3	7.9 [59]	4	2.0
VCeS(c1-i)	18.4		3	2.0
VCeS(c2)	23.5		2	1.6

[a] Feed conditions: methanol:O_2:N_2 = 2:6:30 mL min^{-1}, catalyst loading 0.2 g.
[b] N_s is the number of exposed catalytic active vanadium atoms per square meter supposing that all vanadium atoms are located on the surface and calculated from Table 1.
[c] The theoretical number of exposed vanadium atoms per square meter on TiO_2, ZrO_2, Al_2O_3 and CeO_2 for the monolayer coverage.
[d] TOF of methanol conversion at 393 K.

respectively. This suggests that VTi catalyst mainly possessed strong redox sites, while activities were enhanced with the temperature increase. Upon doping VTi samples with SO_4^{2-}, the selectivity to DMM was greatly improved apparently due to the enhancement of surface acidity with the addition of SO_4^{2-}, while the selectivity to the relative oxidation products (MF and FA) decreased especially for sample VTiS(c2). Moreover, the improved acidity must be mainly due to some medium strength acid sites, since the selectivity to DME (created on the strong acid sites) still remained at a very low level.

With VZr(c1) sample (Fig. 10B), low methanol conversion with high selectivity to DMM was observed up to 423 K. Above this temperature, the selectivity to DMM gradually decreased, whereas the selectivity to MF increased rapidly and became the main product. This observed trend, similar with VTi(c1) sample, can be explained by assuming that a slight increase in quantity of active redox site, and/or the deactivation of a part of medium acidic sites occurred when increasing the reaction temperature. For VZrS samples, the selectivity to DMM was improved by SO_4^{2-} doping but not as much as VTiS samples. In addition, a small amount of DME was also obtained for VZrS samples, suggesting the existence of strong acid sites.

Fig. 10C presents the catalytic performance for VAl and VAlS samples. In the low-temperature range of 393–423 K, sample VAl(c1) yielded mainly DMM with much lower methanol conversion (1–8%) compared to VTi(c1) and VZr(c1) samples. The other possible products (FA, MF and DME) were formed in low amount. The formation of DME is possibly created by the uncovered acidic Al_2O_3 support since pure Al_2O_3 carrier possesses a high activity for dehydration of methanol to DME [55]. With the addition of SO_4^{2-}, the selectivity to DME was obviously increased while the formation of DMM was slightly enhanced, again indicating that the sulfate species located on alumina support favor the dehydration of methanol to DME.

Sample VCe(c1), shown in Fig. 10D, exhibits up to 423 K low conversion of methanol (4–13%) with very high selectivity to DMM (94–99%) and a light selectivity to FA (0–7%). From 423 K, DMM production decreases, again in favor of a high activity and selectivity of oxidation products (FA and MF). Note that the main oxidation products for VCe(c1) sample were FA and not MF. This can be attributed to the high concentration of redox sites and to a lack of acidic sites. Indeed acid sites may enable condensation reactions (Scheme 1) based on the results from H_2–TPR and ammonia adsorption calorimetry measurements.

In summary, we have demonstrated that sample VTiS(c2) prepared simply by straightforward co-precipitation is the best sample for partial oxidation of methanol to DMM, in agreement with a previous paper [57].

As is well known, there are multiple ways in which the host metal oxide may affect the activity of the catalyst. The relatively independent turnover frequency (TOF) values can help in determining the intrinsic activity of these catalysts. The number of exposed surface vanadium active sites was referenced to the N_s (surface vanadium sites per square meter) value of monolayer surface vanadia catalysts (6.8–7.9 V nm^{-2}) [26,34,58,59]. Below monolayer coverage, N_s was simply taken as the number of surface vanadium atoms (see Table 5, column 2). Above monolayer coverage, N_s was taken as the theoretical value of monolayer vanadia coverage (Table 5, column 3). Note that for VCe and VCeS samples, the exposed surface vanadium sites originate from highly dispersed VO_x species (confirmed by Raman spectroscopy) and $CeVO_4$ compound.

As presented in Table 5, the methanol oxidation turnover frequency (TOF) of the surface vanadium sites varies by two orders of magnitude when the metal oxide support is changed from TiO_2 (15.9×10^{-4} s^{-1}) to Al_2O_3 (0.4×10^{-4} s^{-1}). The TOFs of the surface vanadium oxide phase supported on ZrO_2 (4.2×10^{-4} s^{-1}) and CeO_2 (2.0×10^{-4} s^{-1}) have intermediate values. Kim and Wachs [32] have already clarified that surface VO_4 monomers and polymers not crystalline V_2O_5 are the catalytic active sites for methanol oxidation, independently of the VO_4 content, suggesting that this selective oxidation reaction involves only one surface VO_4 site. In addition, Deo and Wachs proposed that the bridging V—O—V bonds and the terminal V=O bonds were not involved in the kinetically relevant rate-determining step. Essentially, in this work, the same isolated and/or polymeric surface VO_4 species were present on the different oxide supports, as confirmed by Raman spectroscopy. This suggests that V—O-support bond could be the key parameter involved in the relevant rate-determining step (Scheme 1) [60].

Another method often used to cast light on the mechanism of catalytic action is to search for correlations between the catalyst reactivity and some other property of its surface. Even if the kinetics of reduction conducted with different reduction agents (H_2 and methanol) can be different, the reducibilities of a series of catalysts have been shown to vary in the same order independently of the reducing agent used [56]. For this reason, correlations between the maximum reduction temperature in H_2-TPR and the catalytic activity can give useful information, as already pointed out by several authors [61,62]. Fig. 11 shows a correlation of the TOF values and the T_{max} data obtained from TPR experiments.

For VM(c1) (M = Ti, Zr, Al and Ce) samples, the T_{max} increases in the order of VAl (796 K) > VCe (790 K) > VZr (742 K) > VTi (708 K), whereas the TOF value presents an opposite trend. This observation reveals that a decrease in the T_{max} temperature would result in an increase in TOF. Furthermore, the T_{max} is related to the reducibility of samples. Although a correlation between catalytic activity in oxidation reaction and reducibility of catalysts has already existed [61,62], the factors determining the reducibility of vanadium species are still unclear. The results of a study [60,63], concluded by TPR, on the reducibility of vanadium oxide catalyst led to the assumption that the reducibility of a catalyst is mainly influenced by vanadia-support interactions. These interactions can be related to the parameter z/a, i.e., the ratio of the carrier charge to the sum of ionic radii of carrier cation and oxide anion [56,64]. As reported in the literature [64], the z/a value of carrier cation increases in the order of V/TiO_2 (1.99) > V/ZrO_2 (1.79) > V/CeO_2 (1.69) > V/Al_2O_3 (1.55). This trend was found to be consistency with the reducibility: higher z/a values correspond to larger reducibility.

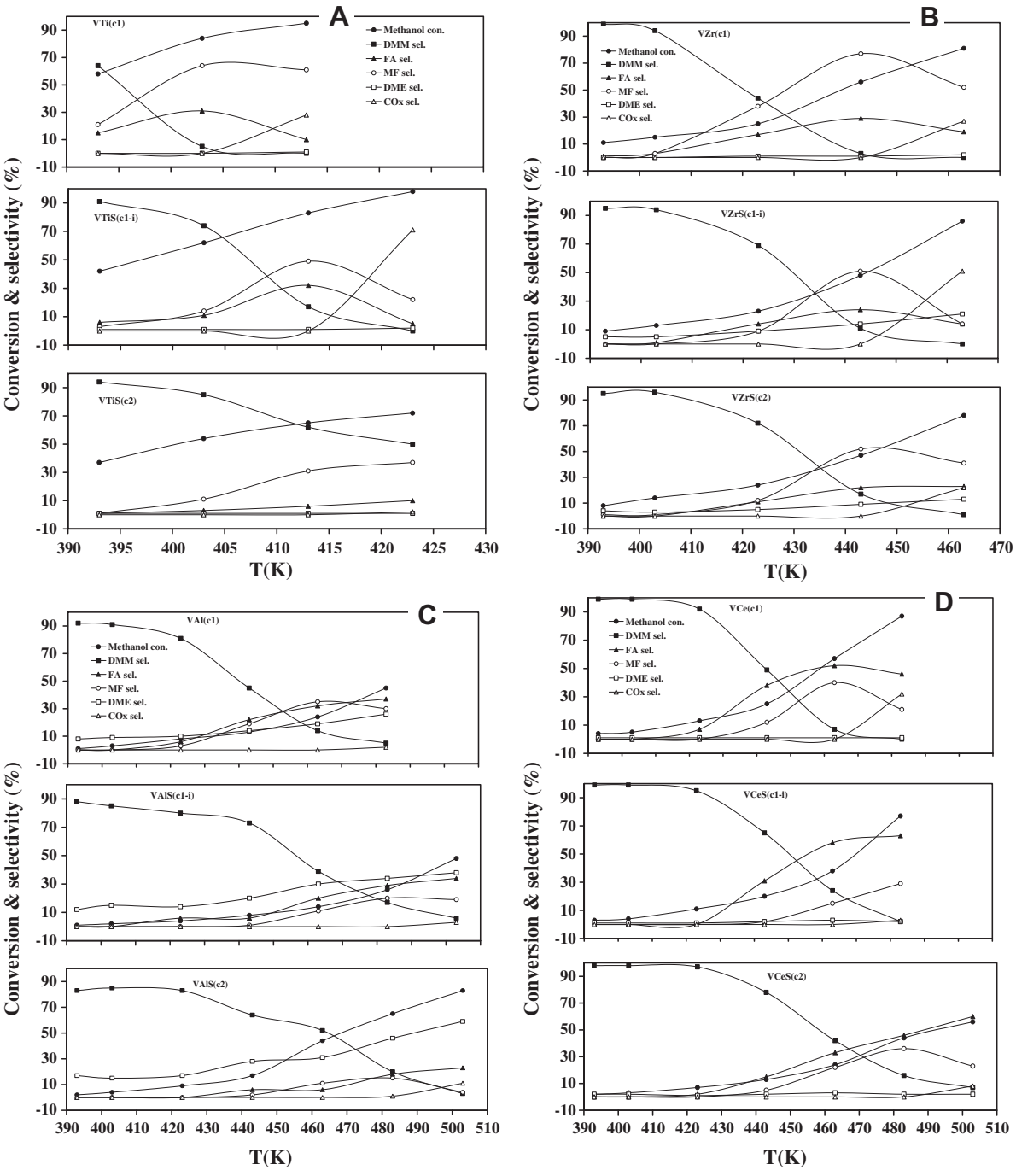

Fig. 10. Selective oxidation of methanol over (A) VTiS samples, (B) VZrS samples, (C) VAlS samples and (D) VCeS samples.

Upon the addition of SO_4^{2-} to VM(c1) (M = Ti, Zr, Al and Ce) samples, the corresponding maximum temperature of TPR peaks (T_{m1} in Table 4) shifted to higher value. Additionally, the T_{m1} value of VMS(c2) samples prepared by simply straightforward co-precipitation is always higher than those of the corresponding VMS(c1-i) samples regardless the concentration of sulfate. Comparing each VMS system, we can found that a higher T_{m1} value is correlated to a lower TOF value except for sample VAlS(c2). As yet no conclusive explanation can be given for this discrepancy. In order to investigate the effect of the strength of sulfate-support interactions on TOFs values, the comparison of systems VM(c1) and VMS(c1-i) was examined. The TOF value of sample VTiS(c1) decreased of 24% compared with sample VTi(c1), while the TOF value of VZrS(c1-i) decreased of 17% compared to VZr(c1). Further, no decrease in TOF values was observed by doping VAl(c1) and VCe(c1) samples with SO_4^{2-}. The decreasing rate of TOF value upon the addition of sulfate species is strongly related to the nature of the metal oxide which controls the type and strength of sulfate species (investigated by TPD–MS and TPR–MS). It has been reported for vanadia–titania samples that the presence of sulfate species could poison the catalytically active sites and then decrease the TOF value [57]. Indeed, the strength of sulfate species determines the number of active sulfate sites on the support. For example, as the strength of the Ti—S bond is weaker (low SO_4^{2-} desorption temper-

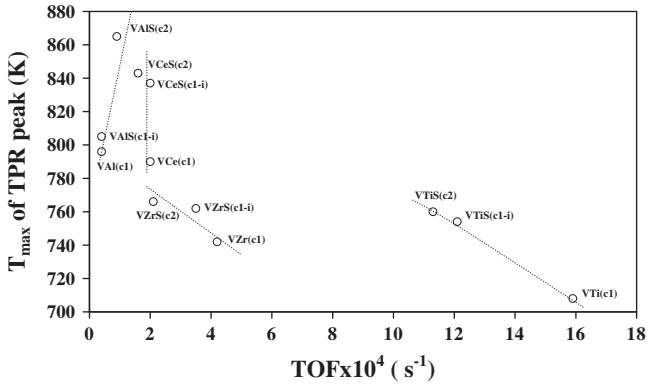

Fig. 11. Correlation between the intrinsic activity of the catalysts relative to TOF value and the maximum temperature of the reduction peak.

ature in Table 3) than the Al—S bond (high SO_4^{2-} desorption temperature), the corresponding SO_4^{2-} sites are in larger number and more poisoning, thus giving rise to a higher decreasing of TOF.

4. Conclusion

The mixed vanadia-based oxides (V_2O_5—TiO_2, V_2O_5—ZrO_2, V_2O_5—Al_2O_3 and V_2O_5—CeO_2) and the corresponding sulfated catalysts were prepared by co-precipitation. Another series of sulfated catalysts was also synthesized by typical incipient wetness impregnation to investigate the effect of preparation method on the strength of sulfate-support interaction. All the studied catalysts with high surface area (73–560 $m^2\ g^{-1}$) and good active phase dispersion were evaluated in partial oxidation of methanol to DMM.

The Raman spectra provided detailed information about the nature of surface metal oxide species: (1) terminal V=O and bridging V—O—V bonds were obtained for all samples except for VAl and VAlS which have no terminal V=O bonds; (2) no V—O-support bridging bond was observed on VTi and VTiS samples due to the incorporation of vanadium in V—O—V bridges; (3) a metal vanadate compound (i.e., $CeVO_4$) formed only on VCe and VCeS samples. The XPS measurements support the stabilization of Ce(III) by $CeVO_4$ formation and reveal no changes in the oxidation state of V(+V). The ammonia adsorption calorimetry study showed a special behavior with weaker adsorption heats at low coverage only for sample VTiS(c1-i) that containing weak sulfate species (bisulfate and/or low polymerized sulfate species) based on the results from TPD–MS. The strength of sulfate-support interactions depends on the nature of the oxide support and increases in the order of VCeS > VAlS > VZrS > VTiS, as indicated by TPD–MS and TPR–MS techniques. Additionally independently of the sulfate concentration, the strength of the sulfate species present on VMS (M = Ti, Zr, Al and Ce) catalysts prepared directly by co-precipitation are stronger than the corresponding samples prepared by impregnation.

The combination of the results obtained from TPR–MS and catalytic test indicates that the reducibility of catalyst determines its catalytic activity. Sample VTi(c1) exhibits the highest TOF value of vanadium site, reflecting the highest activity in methanol oxidation. With the addition of sulfate, the selectivity to DMM was enhanced whereas the TOF value decreased; the decreasing rate of TOF value depending on the strength of sulfate-support interaction. Consequently, sample VTiS(c2) prepared by a simply straightforward co-precipitation exhibited the best catalytic activity for DMM producing, because of the higher reducibility, proper acidity and moderate strength of sulfate species.

Acknowledgments

The authors are thankful to the scientific services of IRCELYON, particularly to Laurence Massin for providing XPS measurements.

Hongying Zhao gratefully acknowledges the China Scholarship Council for the financial support of her PhD grant.

Financial supports from NSFC (20673055) and MSTC (2005CB221400 and 2004DFB02900) are acknowledged.

References

[1] G. Deo, I.E. Wachs, J. Haber, J. Crit. Rev. Surf. Chem. 4 (1994) 141–183.
[2] I.E. Wachs, B.M. Weckhuysen, Appl. Catal. A: Gen. 157 (1997) 67–90.
[3] B.M. Weckhuysen, D.E. Keller, Catal. Today (78) (2003) 25–46.
[4] M.A. Bañares, Catal. Today 51 (1991) 319–348.
[5] V.V. Guliants, Catal. Today 51 (1999) 255–268.
[6] J.N. Al-Saeedi, V.V. Guliants, O. Guerrero-Pérez, M.A. Bañares, J. Catal. 215 (2003) 108–115.
[7] F. Trifiro, B. Grzybowska, Appl. Catal. A: Gen. 157 (1997) 1–2.
[8] C.N. Satterfield, Heterogeneous Catalysis in Practice, McGraw-Hill, New York, 1980.
[9] L. Owens, H.H. Kung, J. Catal. 144 (1993) 202–213.
[10] F. Arena, F. Frusteri, A. Parmaliana, Appl. Catal. A: Gen. 176 (1999) 189–199.
[11] J.M. Tatibouët, Appl. Catal. A: Gen. 148 (1997) 213–252.
[12] P. Forzatti, E. Tronconi, A.S. Elmi, G. Busca, Appl. Catal A: Gen. 157 (1997) 387–408.
[13] M.D. Amiridis, I.E. Wachs, G. Deo, J.M. Jehng, D.S. Kim, J. Catal. 161 (1996) 247–253.
[14] H. Liu, E. Iglesia, J. Catal. 223 (2004) 161–169.
[15] H. Liu, P. Cheung, E. Iglesia, J. Catal. 217 (2003) 222–232.
[16] J.M. Tatibouët, H. Lauron-Pernot, J. Mol. Catal. A: Chem. 171 (2001) 205–216.
[17] Y. Fu, J. Shen, Chem. Commun. 21 (2007) 2172–2174.
[18] H. Zhao, S. Bennici, J. Shen, A. Auroux, Appl. Catal. A: Gen. 356 (2009) 121–128.
[19] P. Malet, A. Caballero, J. Chem. Soc., Faraday Trans. I 84 (1988) 2369–2375.
[20] D.A.M. Monti, A. Baiker, J. Catal. 83 (1983) 323–335.
[21] P. Schneider, Appl. Catal. A: Gen. 129 (1995) 157–165.
[22] F.D. Hardcastle, I.E. Wachs, J. Phys. Chem. 95 (1991) 5031–5041.
[23] J.P. Dunn, J-M. Jehng, D.S. Kim, L.E. Briand, H.G. Stenger, I.E. Wachs, J. Phys. Chem. B 102 (1998) 6212–6218.
[24] J. Twu, P.K. Dutta, J. Catal. 124 (1990) 503–510.
[25] S.T. Choo, Y.G. Lee, I.S. Nam, S.W. Ham, J.B. Lee, Appl. Catal. A: Gen. 200 (2000) 177–188.
[26] I.E. Wachs, Catal. Today 27 (1996) 437–455.
[27] X. Gao, M.A. Bañares, I.E. Wachs, J. Catal. (188) (1999) 325–331.
[28] N. Magg, B. Immaraporn, J.B. Giorgi, T. Schroeder, M. Bäumer, J. Döbler, Z. Wu, E. Kondratenko, M. Cherian, M. Baerns, P.C. Stair, J. Sauer, H.J. Freund, J. Catal. 226 (2004) 88–100.
[29] H. Tian, E.I. Ross, I.E. Wachs, J. Phys. Chem. B 110 (2006) 9593–9600.
[30] M.A. Vuurman, I.E. Wachs, J. Phys. Chem. 96 (1992) 5008–5016.
[31] M.A. Vuurman, I.E. Wachs, J. Mol. Catal. 77 (1992) 29–39.
[32] T. Kim, I.E. Wachs, J. Catal. 255 (2008) 197–205.
[33] M.V. Martinez-Huerta, G. Deo, J.L.G. Fierro, M.A. Bañares, J. Phys. Chem. C (111) (2007) 18708–18714.
[34] B.M. Reddy, A. Khan, Y. Yamada, T. Kobayashi, S. Loridant, J.C. Volta, J. Phys. Chem. B 107 (2003) 5162–5167.
[35] J. Matta, D. Courcot, E. Abi-Aad, A. Aboukaïs, Chem. Mater. 14 (2002) 4118–4125.
[36] V.I. Bukhtiyarov, Catal. Today 56 (2000) 403–413.
[37] M.H. Kim, I.S. Nam, Y.G. Kim, J. Catal. 179 (1998) 350–360.
[38] J.P. Chen, R.T. Yang, J. Catal. (139) (1993) 277–288.
[39] B.M. Reddy, A. Khan, Y. Yamada, T. Kobayashi, S. Loridant, J.C. Volta, J. Phys. Chem. B (106) (2002) 10964–10972.
[40] D.R. Mullins, S.H. Overbury, D.R. Huntley, Surf. Sci. 409 (1998) 307–319.
[41] D.A. Creaser, P.G. Harrison, M.A. Morris, B.A. Wolfindale, Catal. Lett. 23 (1994) 13–24.
[42] J.Z. Shyu, W.H. Weber, H.S. Gandhi, J. Phys. Chem. 92 (1988) 4964–4970.
[43] A. Auroux, Top. Catal. 4 (1997) 71–89.
[44] H. Zhao, S. Bennici, J. Shen, A. Auroux, J. Therm. Anal. Calorim. 99 (2010) 843–847.
[45] A. Desmartin-Chomel, J.L. Flores, A. Bourane, J. M Clacens, F. Figueras, G. Delahay, A. Giroir Fendler, C. Lehaut-Burnouf, J. Phys. Chem. B 110 (2006) 858–863.
[46] R.L. White, E.C. Sikabwe, M.A. Coelho, D.E. Resasco, J. Catal. 157 (1995) 755–758.
[47] M. Waqif, O. Saur, J.C. Lavelley, Y. Wang, B.A. Morrow, Appl. Catal. 71 (1991) 319–331.
[48] I.E. Wachs, J. Catal. 124 (1990) 570–573.
[49] G.Y. Popova, T.V. Andrushkevich, E.V. Semionova, Y.A. Chesalov, L.S. Dovlitova, V.A. Rogov, V.N. Parmon, J. Mol. Catal. A: Chem. 283 (2008) 146–152.
[50] B.Q. Xu, W.M.H. Sachtler, J. Catal. 167 (1997) 224–233.
[51] E. Ghedini, M. Signoretto, F. Pinna, G. Cerrato, C. Morterra, Appl. Catal. B: Environ. 67 (2006) 24–33.
[52] E.A. Mamedov, V. Cortes Corberan, Appl. Catal. A: General 157 (1997) 117–142.

[53] M.V. Martínez-Huerta, J.M. Coronádo, M. Fernandez-García, A. Iglesias-Juez, G. Deo, J.L.F. Fierro, M.A. Bañares, J. Catal. 225 (2004) 240–248.
[54] C.M.S. Polato, C.A. Henriques, A.A. Neto, J.L.F. Monteiro, J. Mol. Catal. A: Chem. 241 (2005) 184–193.
[55] J.B. Laizet, A.K. Soiland, J. Leglise, J.C. Duchet, Top. Catal. 10 (2000) 89–97.
[56] F. Roozeboom, P.D. Cordingley, P.J. Gellings, J. Catal 68 (1981) 464–472.
[57] H. Zhao, S. Bennici, J. Shen, A. Auroux, J. Catal. 272 (2010) 176–189.
[58] A.A. Lemonidou, L. Nalbandian, I.A. Vasalos, Catal. Today 61 (2000) 333–341.
[59] L.E. Briand, O.P. Tkachenko, M. Guraya, X. Gao, I.E. Wachs, W. Grünert, J. Phys. Chem. B 108 (2004) 4823–4830.
[60] I.E. Wachs, Catal. Today 100 (2005) 79–94.
[61] G. Deo, I.E. Wachs, J. Catal. 146 (1994) 323–334.
[62] G. Deo, I.E. Wachs, J. Catal 129 (1991) 307–312.
[63] F. Roozeboom, M.C. Mlttelmeijer-Hazeleger, J.A. Moulijn, J. Medema, V.H.J. de Beer, P.J. Gellngs, J. Phys. Chem. 84 (1980) 2783–2791.
[64] F. Roozeboom, T. Fransen, P. Mars, P.J. Gellngs, Z. Anorg. Allg. Chem. 449 (1979) 25.